Plasma-based electroacoustic transducers
Corona discharge transducer
Sound generation and control

Stanislav Sergeev

Acoustic group of signal processing laboratory LTS2, EPFL, Lausanne

EPFL

Outline

- Introduction
- Plasma-based transducers, properties and problems
- Corona discharge actuator
- Sound sources in corona discharge actuator
- Sound control with corona discharge actuator

Acoustic noise

Observations:

- Environmental noise increases
- Harmful effect of noise is established
- New strict noise management rules in Europe
- Noise becomes more difficult to tackle

Conclusion:

New noise reduction methods are needed

Noise reduction in aircraft engines

- Acoustic liners installed in engine nacelle
- Should be relatively thin, a few centimeters
- Should be very efficient – limited area available

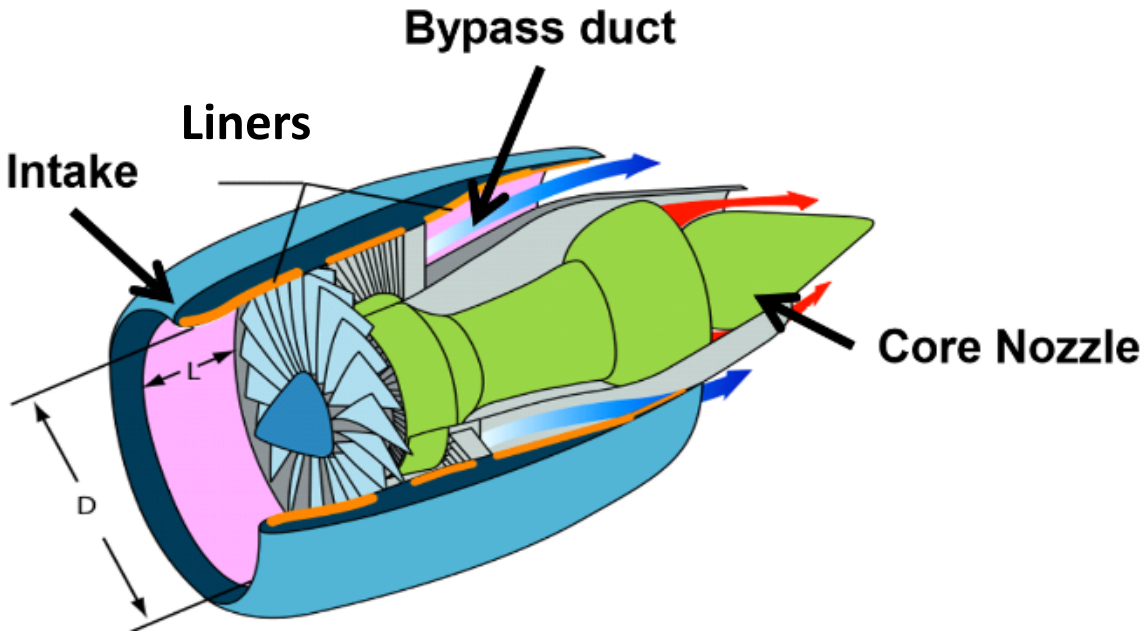

Liners location in engine

Noise reduction – passive methods

Porous absorbers:

+ Broadband performance
- Large size to reduce low frequency noise
- Difficult to install in space limited environment

Resonant absorbers:

+ Can tackle low frequency noise
- Narrowband performance
- Not possible to adjust

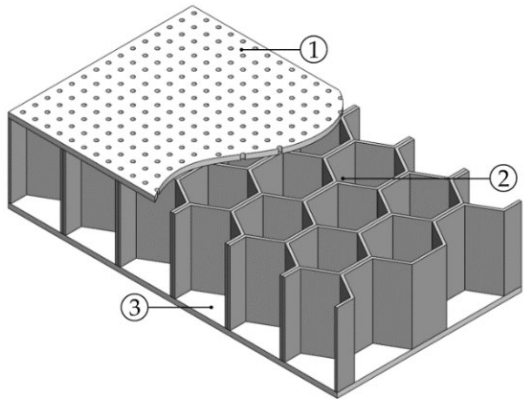

Porous and resonant passive absorbers [1]

[1] Dannemann, M. et al. (2018). Experimental Study of Advanced Helmholtz Resonator Liners with Increased Acoustic Performance by Utilising Material Damping Effects.

Noise reduction – active methods

Active noise cancellation:

- Difficult to install in complex environments

Active sound absorption:

- Wider range of absorption
- Possible to tune range of absorption

Space for further research:

- Compliance to harsh environment
- Weight of the system (in arrays)
- Limited bandwidth of operation

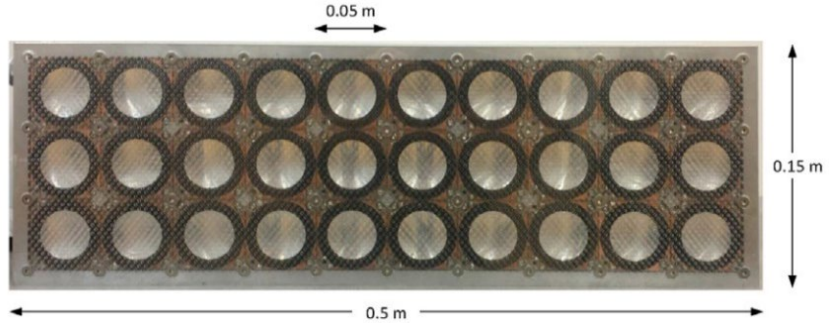

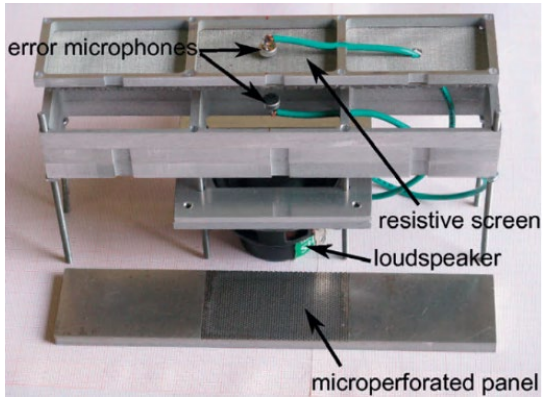

Various prototypes of active absorbers [2,3,4]

[2] Boulandet , R. et al (2018). Duct modes damping through an adjustable electroacoustic liner under grazing incidence.

[3] Betgen, B. et al (2012). Implementation and non-intrusive characterization of a hybrid active – passive liner with grazing flow.

[4] Billon, K. et al (2022). In flow acoustic characterisation of a 2D active liner with local and non local strategies.

Active absorption with electrodynamic loudspeaker

- Acoustic impedance control to absorb sound
- Common transducer for control – electrodynamic speaker
- Passive acoustic impedance $Z(\omega) = j\omega M + R + \frac{1}{j\omega C}$
- Often constant value of impedance is needed to absorb sound
- Moving mass limits high frequency range

Alternative actuator for active control is needed

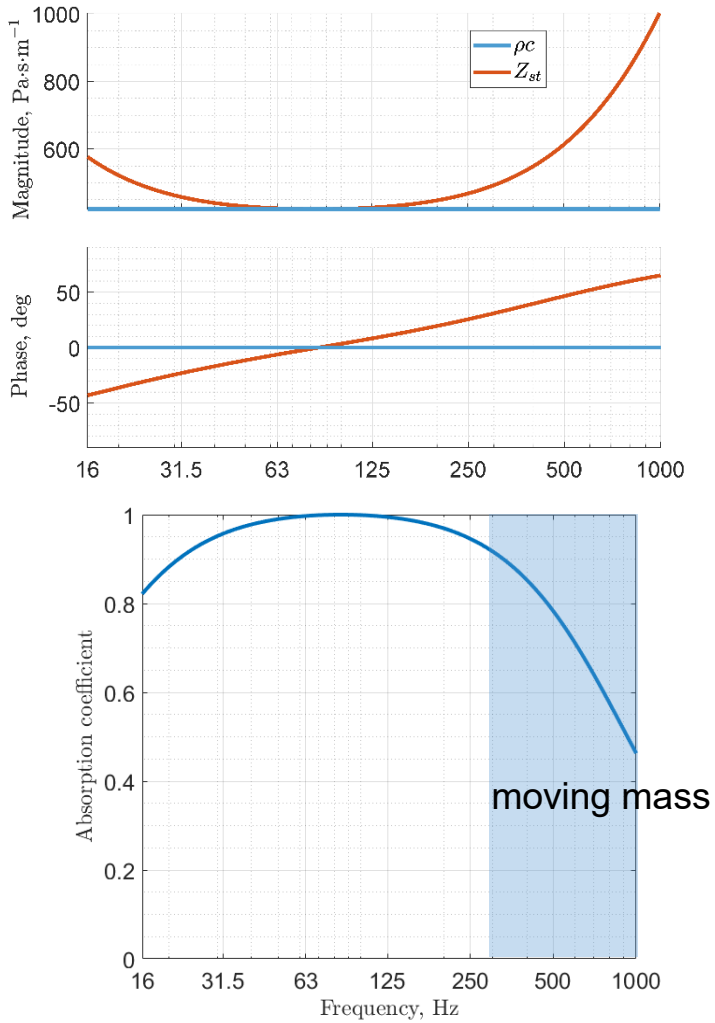

Acoustic impedance and sound absorption with a loudspeaker under normal incidence [5]

[5] Rivet, E. et al (2016). Broadband Low-Frequency Electroacoustic Absorbers Through Hybrid Sensor-/Shunt-Based Impedance Control.

What is needed from the actuator

Develop an electroacoustic actuator for active sound control:

- Lightweight
- Mechanically robust
- Does not present resonant response
  - Has minimal moving mass
- Flexible design

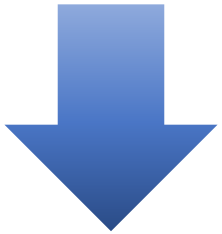

plasma-based actuator

Plasma can make sound, part 1

- What are the properties of the sound?

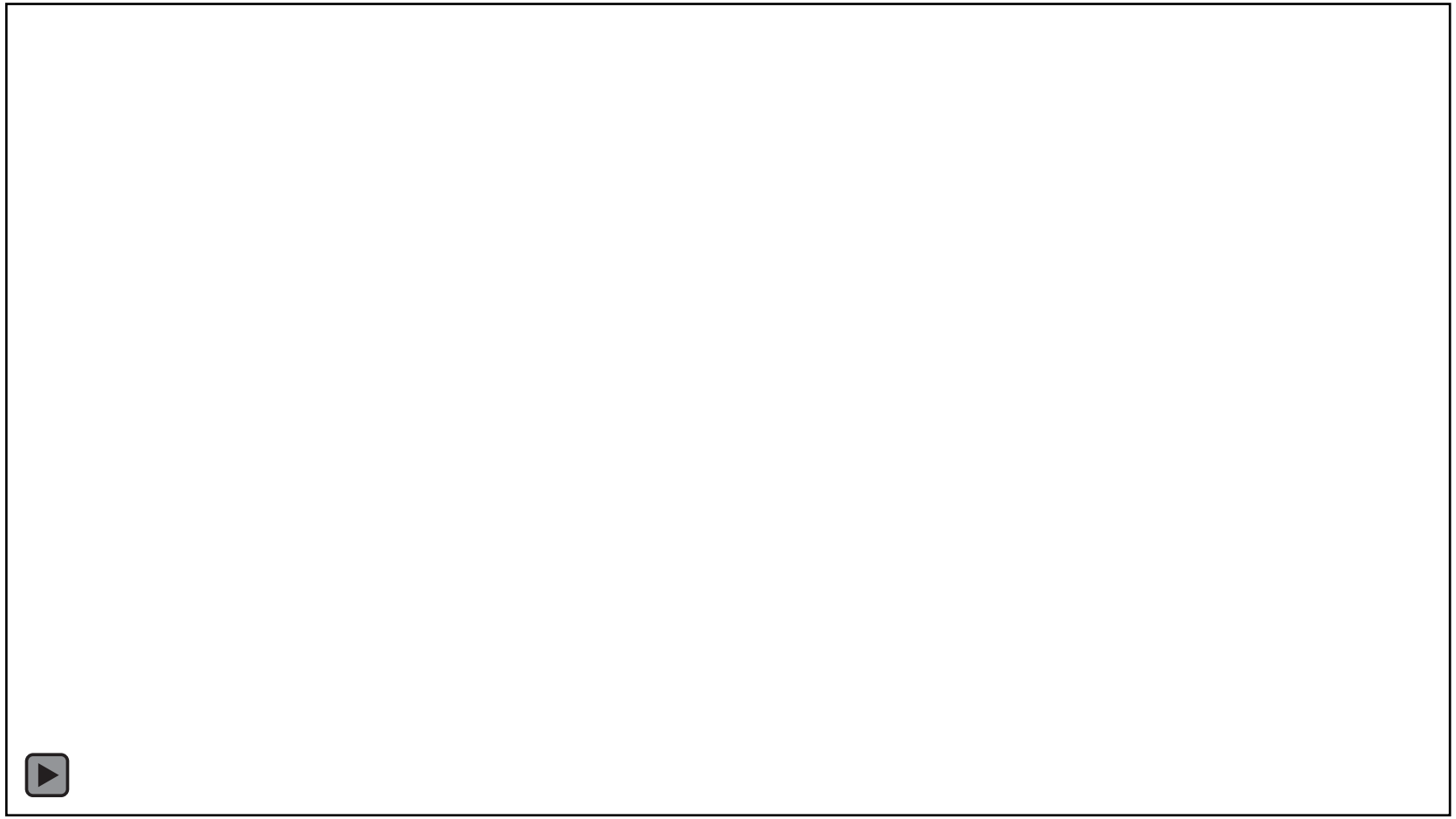

https://www.youtube.com/watch?v=gqs8bRMhBgA

Plasma can make sound, part 2

- What are the features of this sound source?

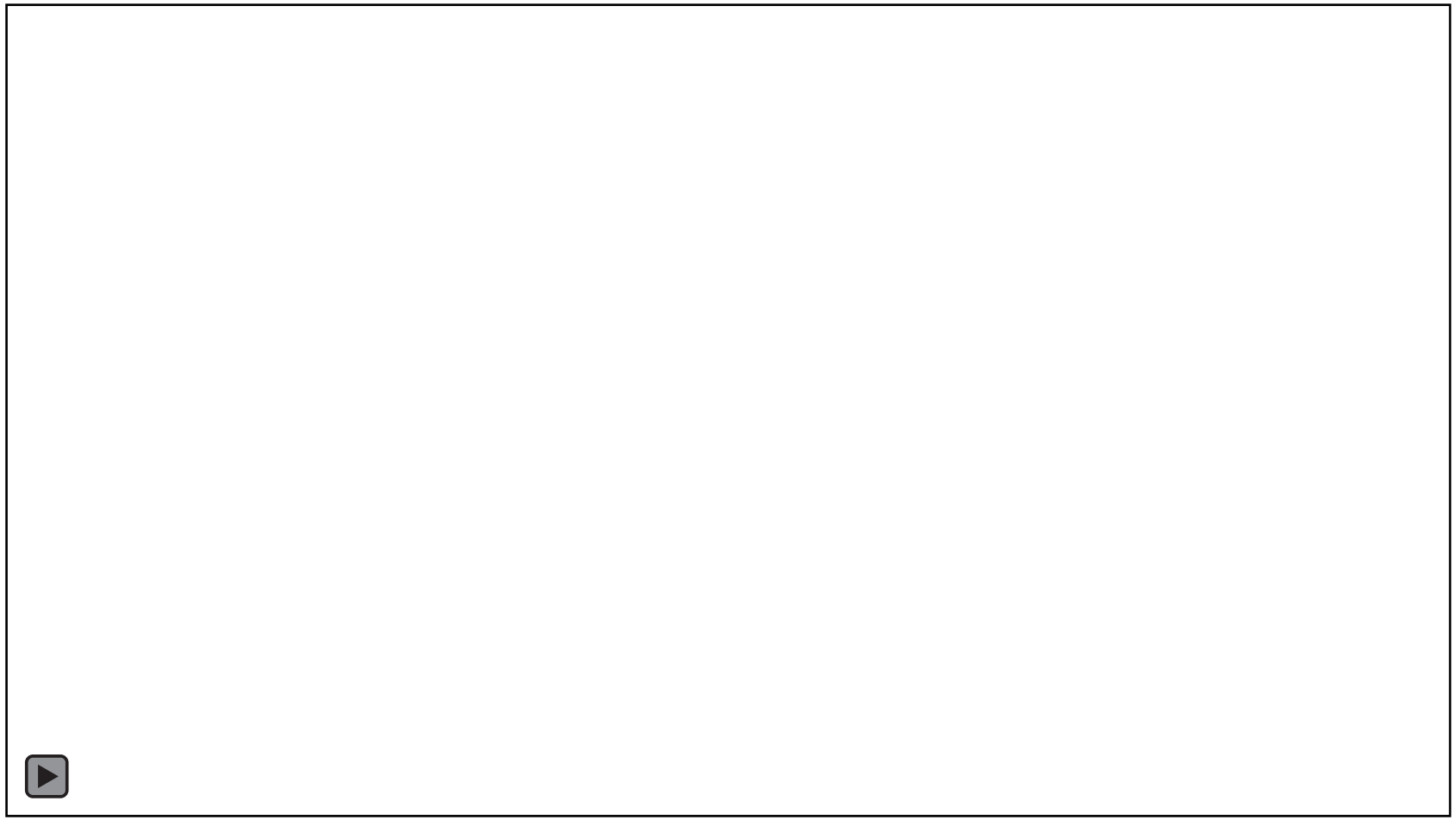

Plasma-based transducers

Acoustic field control via interaction of plasma and medium

Hot plasma transducers

- Electrical arc, HF discharge, streamers
- Sound due to heat transfer from a discharge
- Small size of the discharge region – point source

Cold plasma transducers

- Dielectric barrier discharge (DBD), corona discharge (CD)
- Sound due to elastic interaction of ions and air + heat
- Can be arranged over an extended surface
- DBD is nonlinear

Corona discharge is the most suitable

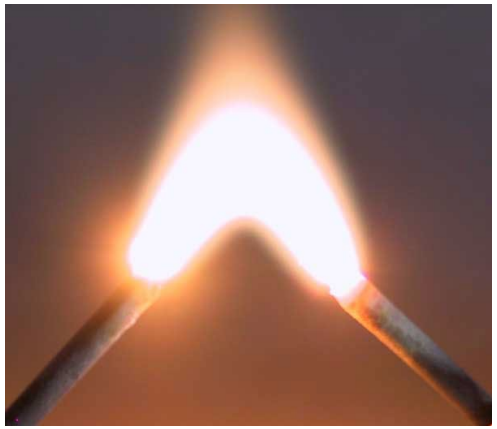

Electric arc plasma

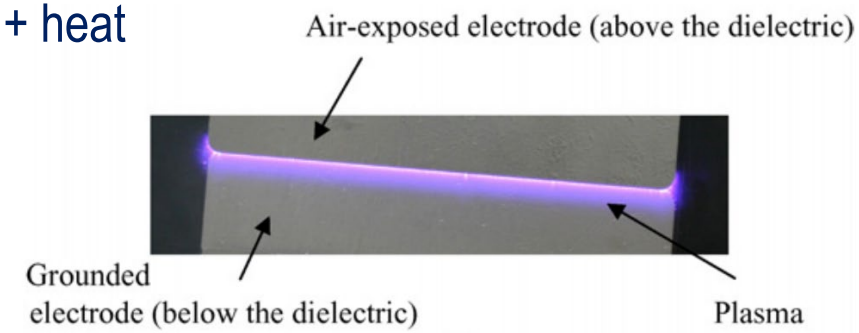

Dielectric barrier discharge [6]

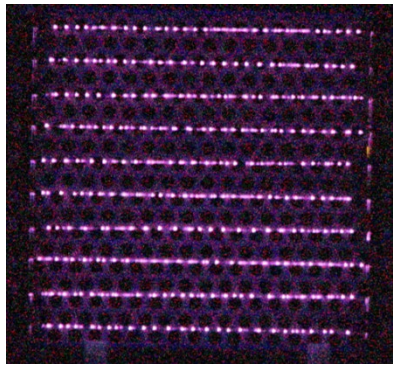

Corona discharge

[6] Moreau, E. (2007). Airflow control by non-thermal plasma actuators.

Dielectric barrier discharge

Geometry:

- 2 flat electrodes
- Strong dielectric separation

Formation:

- High electric field at the edge of the electrode
- Nanosecond streamer formation
- No continuous current

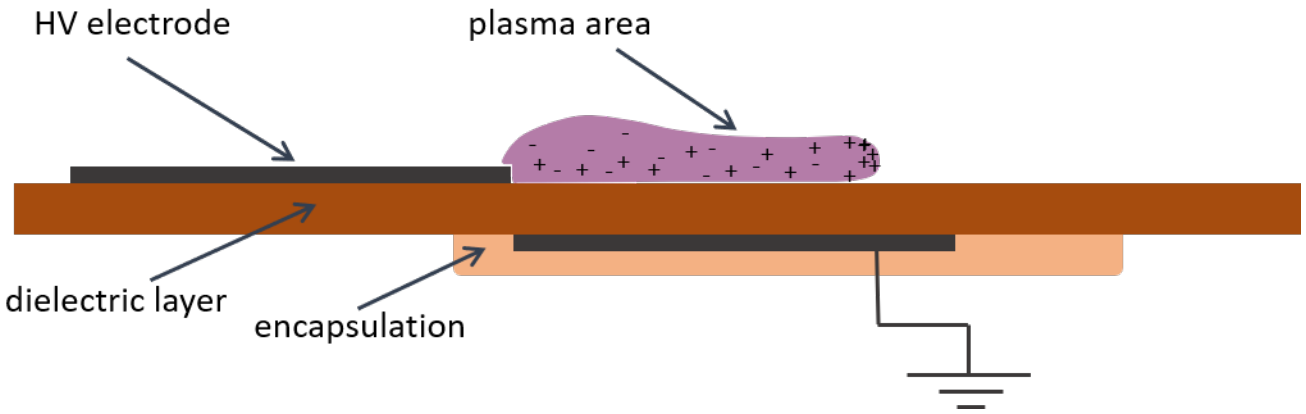

Schematic of the dielectric barrier discharge

Dielectric barrier discharge

Experiment:

- 2 DBD samples tested
- 8 kV 200 ns pulse at f_0=1 kHz
- 8 kV AC voltage at f_0=1 kHz

Results:

- Harmonics $f = n \times f_0$ observed
- High nonlinearity of transducer

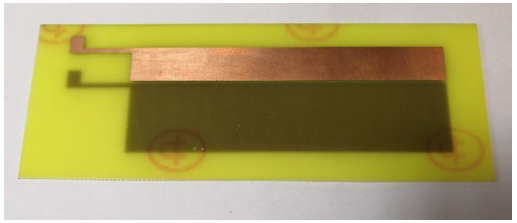

Photo of DBD sample

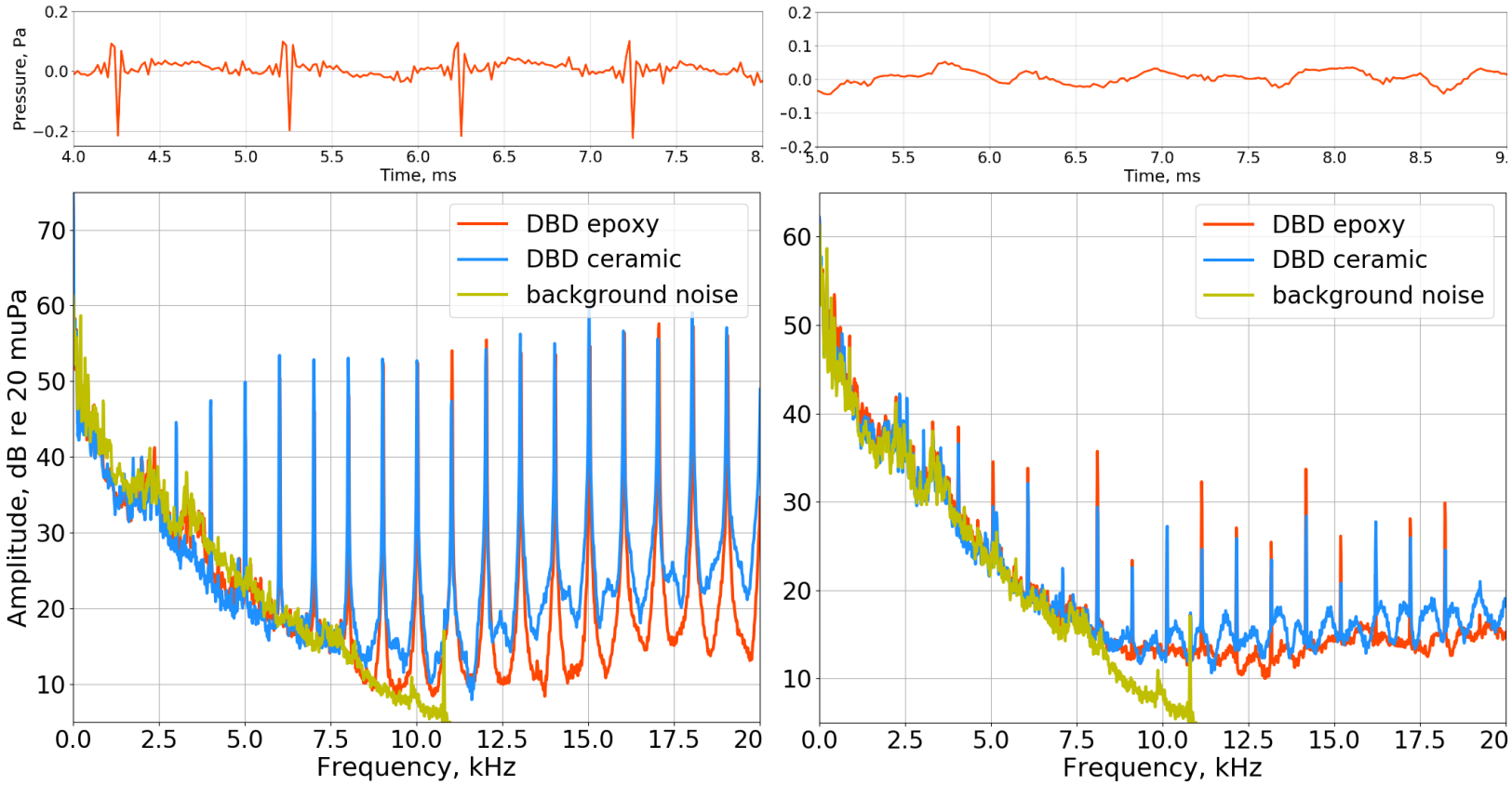

Time series and power spectral density of pressure signal from DBD samples.
Left – nanosecond pulse, right – AC voltage excitation

Corona discharge

Elements of construction

- High curvature emitter (E)
- Smooth and large collector (C)
- Electrode distance ≫ $R_{emitter}$

Corona features

- Continuous current discharge
- Constant air flow velocity at U=U_{DC}=const
- Sound wave generation at U_{DC}+$u_{AC}(t)$
- Can be designed visually transparent
- Arbitrary shape of electrodes

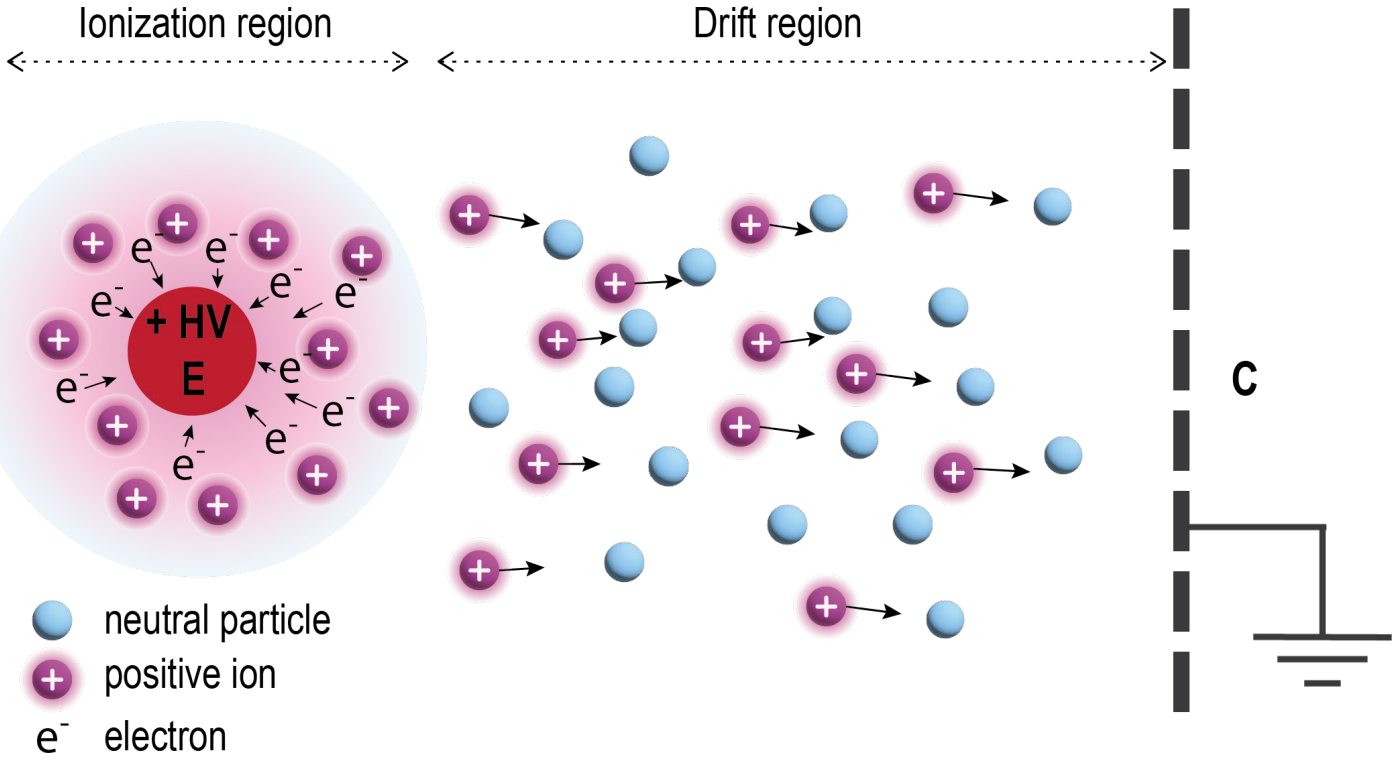

Mechanism of a corona discharge

Geometry of corona discharge transducer

Geometry

- HV electrode – array of thin cylindrical wires
- Collector electrode – conducting grid
- Emitter plane parallel to collector plane

Benefits

- Surface distributed source
- Electrical field from flat capacitor
- Homogeneous flow velocity

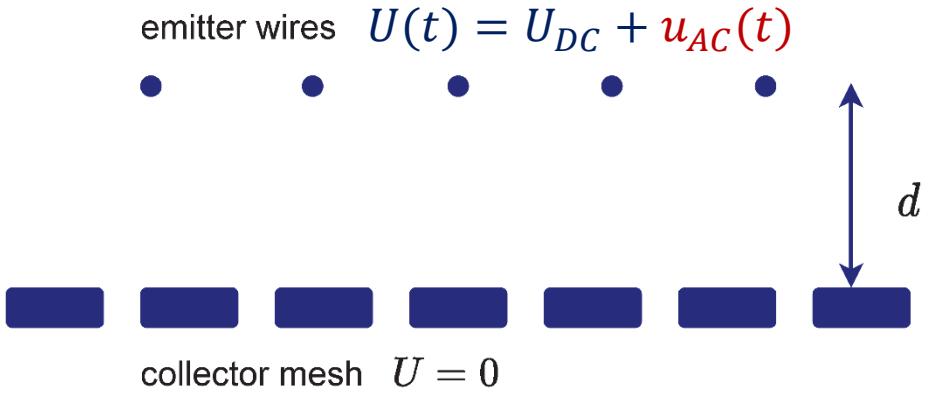

Schematic of a wire-to-mesh CD geometry.
Cross-sectional view

Corona discharge transducer prototype

Materials

- Emitter – 0.1 mm wire
- Collector – smooth perforated metallic plate
- Frame – dielectric material

Dimensions

- 5x5 cm operational area
- 6 mm distance between electrodes
- 10 mm between emitter wires

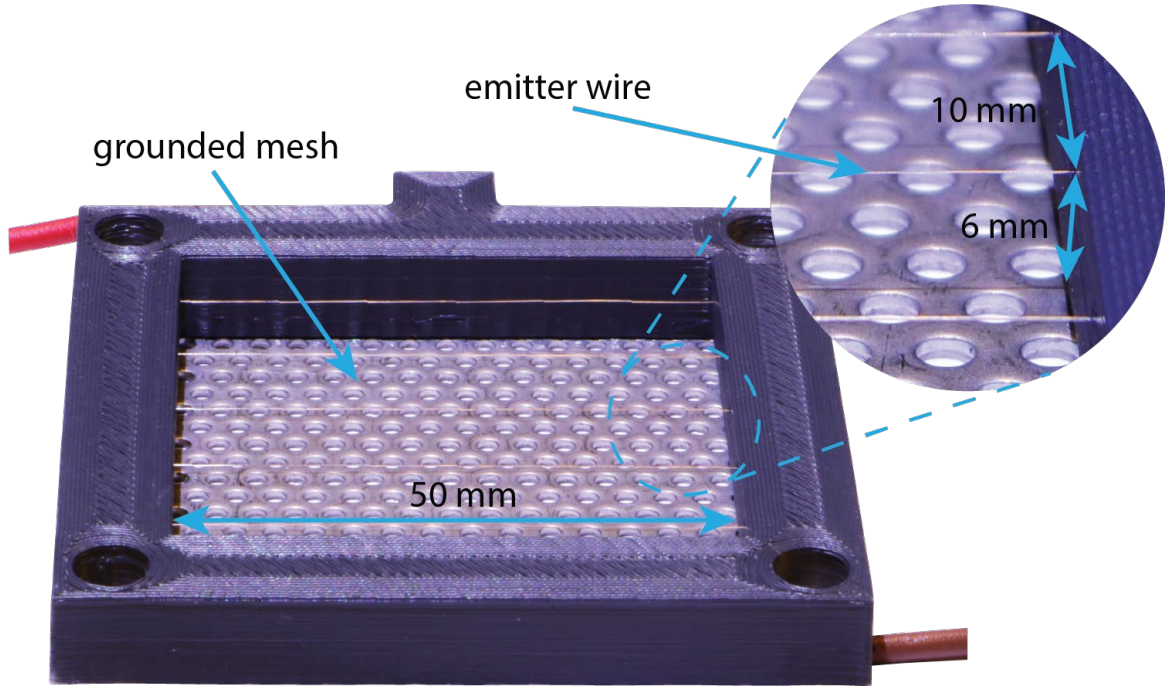

CD actuator used in the experiments

Voltage-current characteristics

- Nonlinear $\mathrm{I}(U)$ dependence
- No current below $U = U_0$
- $I = CU(U - U_0)$ Townsend formula [7] approximates the curve

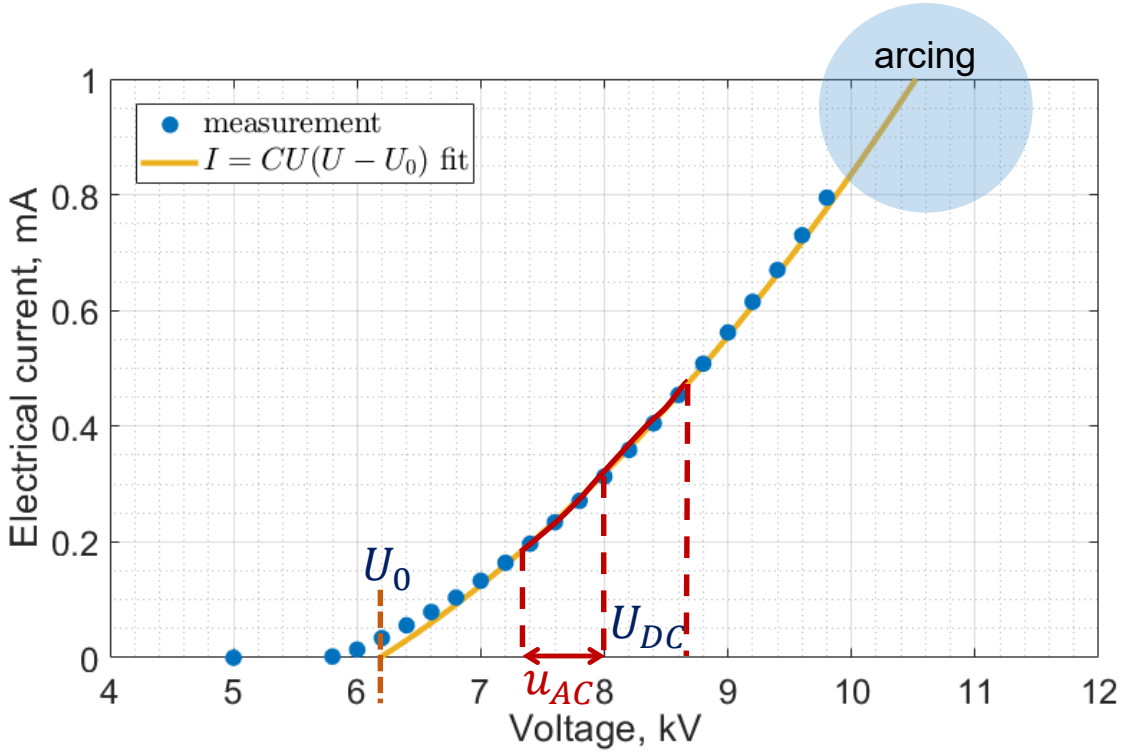

Example of a voltage-current curve of corona discharge

[7] Raizer, Y. P. Gas discharge physics. 1991.

Analytical model – governing equations

Governing equations

$$\frac{\partial \delta}{\partial t} + \rho_0 \nabla \cdot \mathbf{u} = 0$$

$$\rho_0 \frac{\partial \mathbf{u}}{\partial t} + \nabla p = \mathbf{f}$$

$$\rho_0 T_0 \frac{\partial s}{\partial t} = \mathrm{h}$$

$$\delta = \frac{1}{c^2} p - \frac{\rho_0}{C_P} s$$

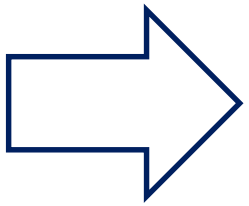

Wave equation with heat and force sources

$$(k^2 + \nabla^2) p = -\frac{j\omega(\gamma - 1)}{c^2} \mathrm{h} + \nabla \cdot \mathbf{f}$$

Solution

$$p(\mathbf{r}) = p_{\mathrm{h}}(\mathbf{r}) + p_{\mathbf{f}}(\mathbf{r})$$

$$p_{\mathrm{h}}(\mathbf{r}) = -\frac{j\omega(\gamma - 1)}{4\pi r c^2} \left(\iiint \mathrm{h} dv_0 \right) \exp(jkr)$$

$$p_{\mathbf{f}}(\mathbf{r}) = -\frac{jk}{4\pi r} \left(\frac{j}{kr} + 1 \right) \left(\iiint \mathrm{f} dv_0 \right) \cos\theta \exp(jkr)$$

Analytical model – heat and force sources

Source estimations

- Heat source – Joule losses
- Force – Coulomb force on ions
- Measurement of I(U) curve is needed + $I = CU(U - U_0)$ approximation

Benefits

- Simple model calibration
- Can obtain frequency response and directivity at low frequencies

$$F_\omega = \iiint \mathrm{f} dv_0 \qquad H_\omega = \iiint \mathrm{h} dv_0$$

Heat source

$$H(t) = U(t)I(t)$$

$$H_\omega = C(3U_{DC}^2 - 2U_{DC}\,U_0)u_{AC}$$

Force source

$$F(t) = \iiint \rho_i(t)E(t)dv_0 = \frac{I(t)d}{\mu_i}$$

$$F_\omega = \frac{Cd}{\mu_i}(2U_{DC} - U_0)u_{AC}$$

Setup for measurements

- Free field in anechoic chamber (cut off 80 Hz)
- Microphone 1 m from CD at the same height
- Turntable for directivity measurement
- TREK 615-10 as HV amplifier
- CD biased at U_{DC}=8 kV

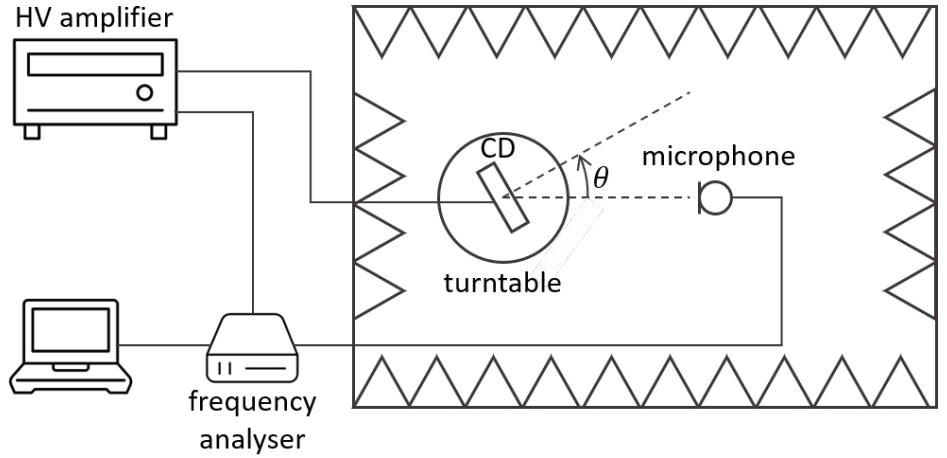

Schematic of free-field acoustic measurements with CD actuator

On-axis frequency response

- 6 dB/octave slope at low frequencies
- Behaves as ideal monopole/dipole
- Analytical model aligns well up to 4 kHz
- Numerical curve 1-2 dB lower
- Numerical model follows at higher frequencies
- Heat and force sources separation can be neglected

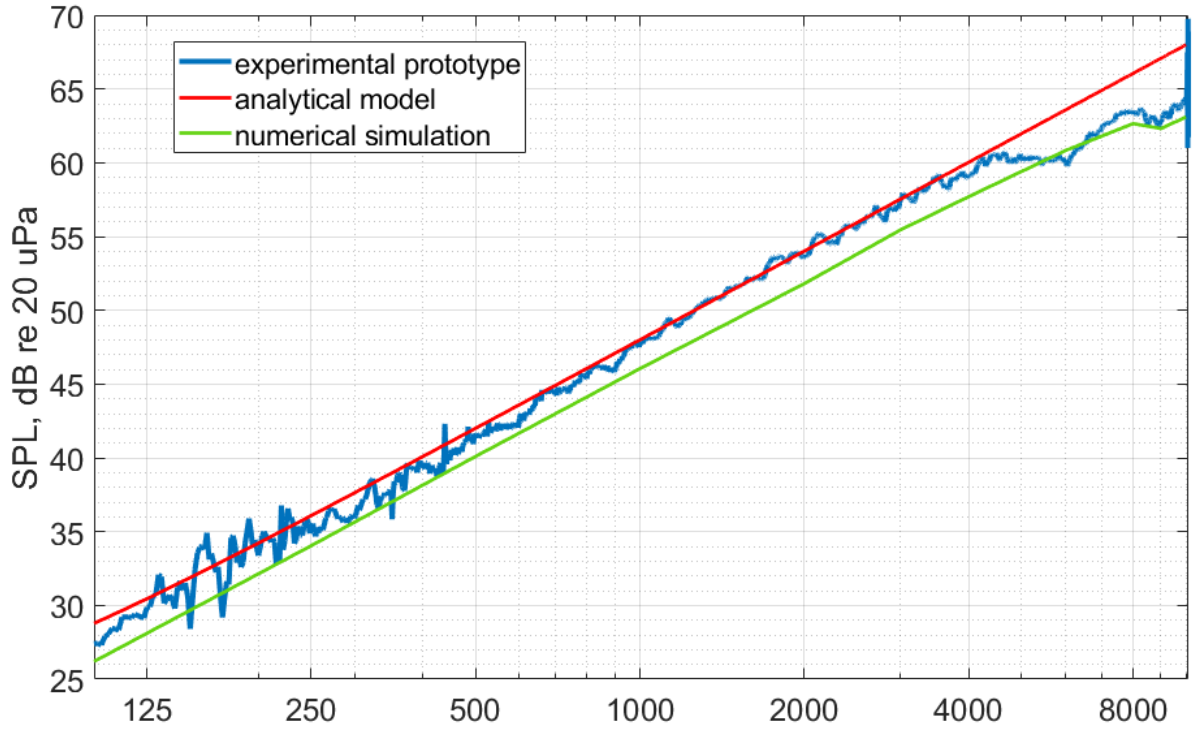

Sound pressure levels measured experimentally and estimated with analytical and numerical models

Directivity patterns

- Supercarioid shape
- Dipolar source is 4.4 times stronger than monopolar
- At high frequencies secondary lobes appear
- Analytical model shows only ideal sources
- Numerical model helps at high frequencies

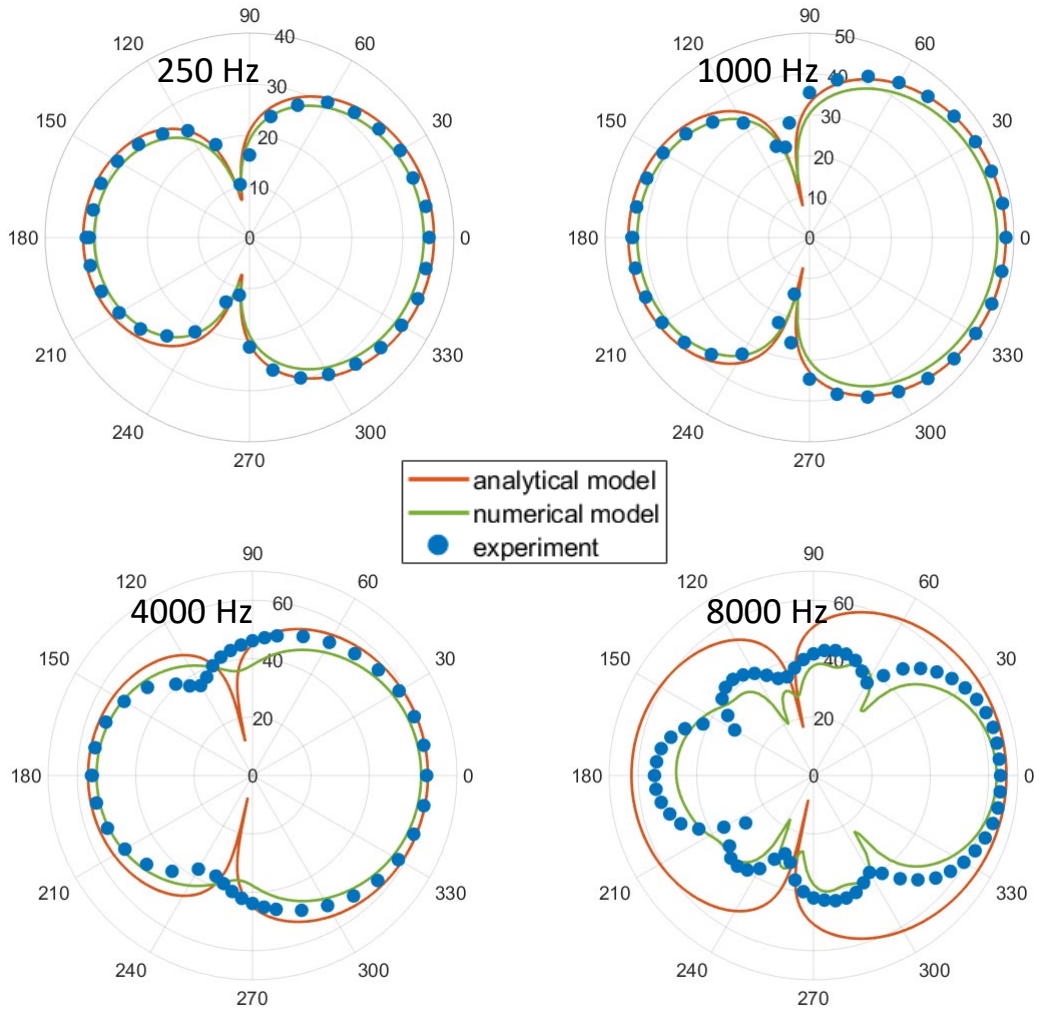

Directivity patterns measured experimentally and estimated with analytical and numerical models

Total harmonic distortion (THD)

- Linear increase of THD with u_{AC} magnitude
- Lower than 10 % at high u_{AC} values (with Lab amp)
- Can be reduced with current control [9]
- No clear dependence on frequency
- Analytical model shows linear dependence on u_{AC}
- Second harmonic dominates in THD

$$THD = 100\sqrt{\frac{\sum_{n=2}^{\infty} A_n^2}{A_1^2 + \sum_{n=2}^{\infty} A_n^2}}$$

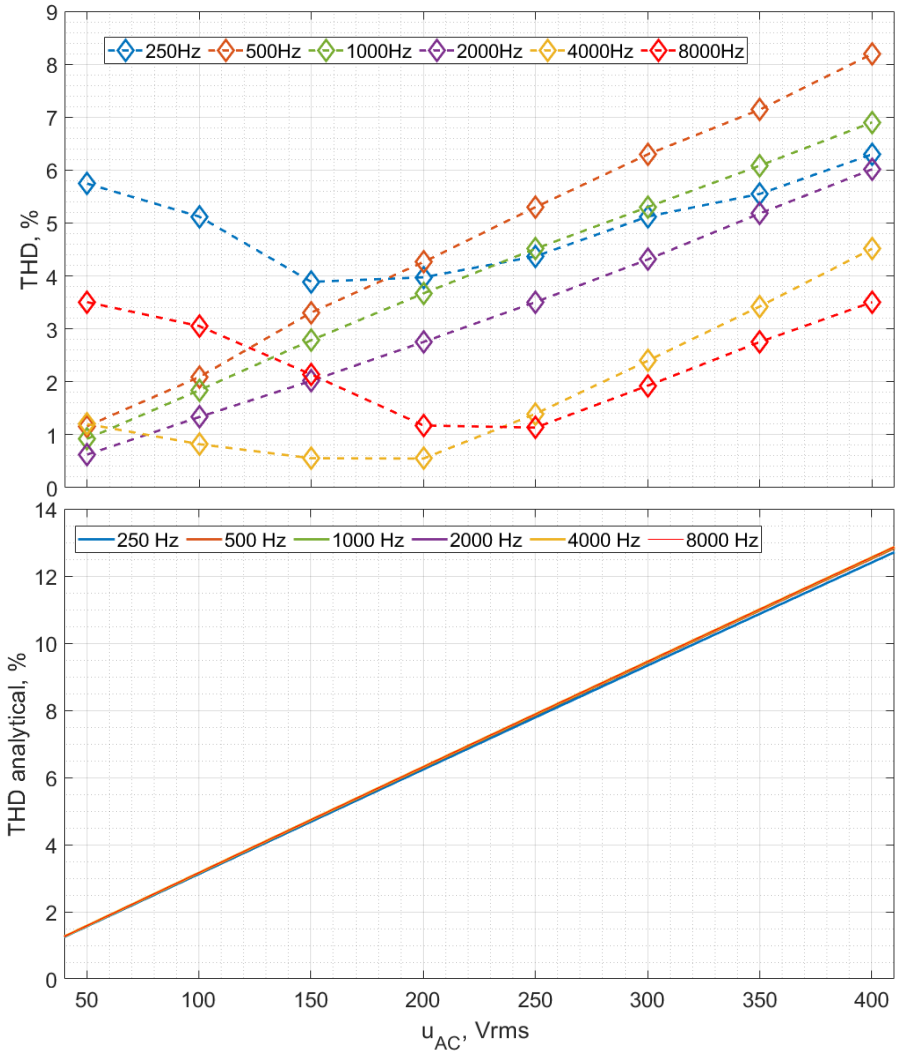

Total harmonic distortion measured experimentally and estimated with analytical model

[9] Béquin, P. et al (2007). Modelling plasma loudspeakers.

Transient response of CD actuator

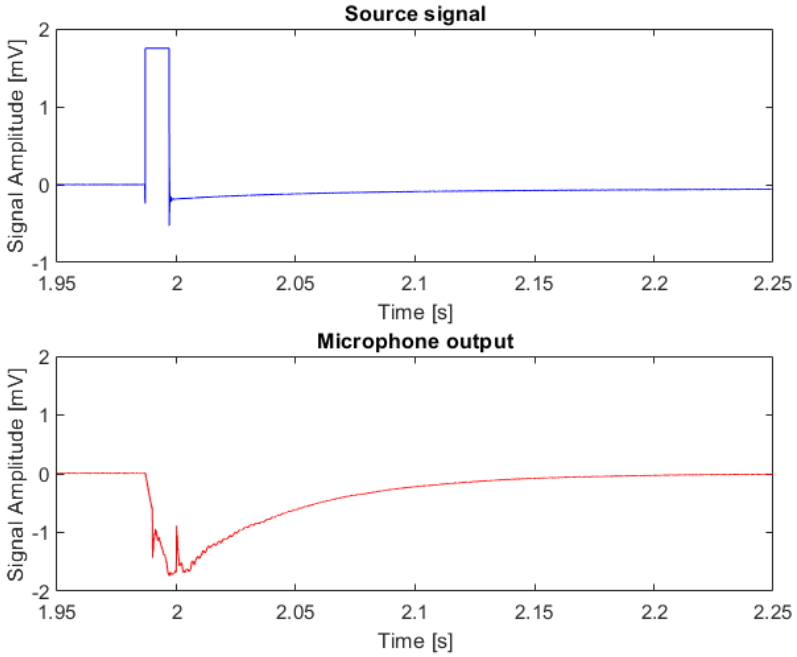

(a) Electrodynamic loudspeaker

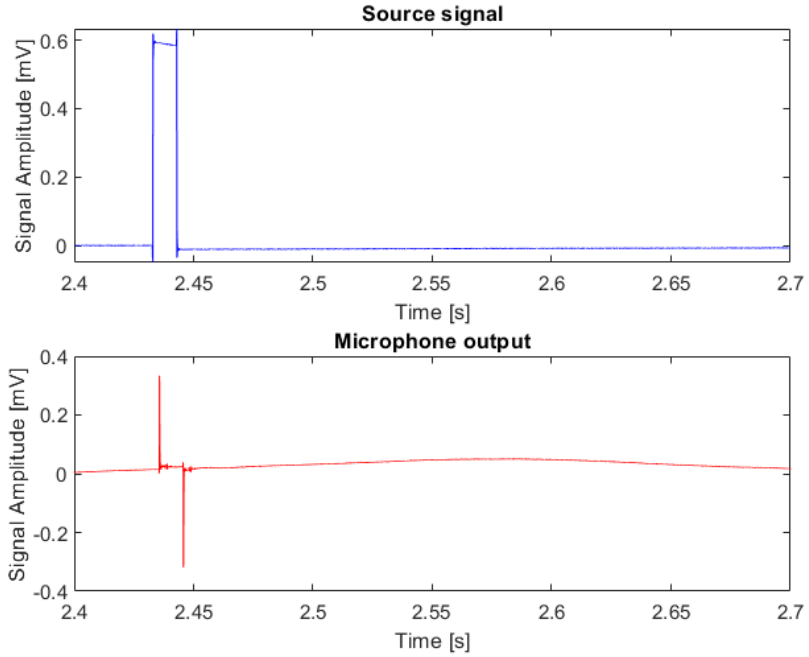

(b) Corona discharge actuator

Principle of absorption with CD actuator

Passive CD

- Electrodes transparent to sound
- Rigid enclosure
- Ideally fully reflective interface

Active CD:

- Transparent electrodes + rigid enclosure
- Force and heat sources of pressure
- Sources can be adjusted to absorb sound
- Analytical estimation of sources can be used

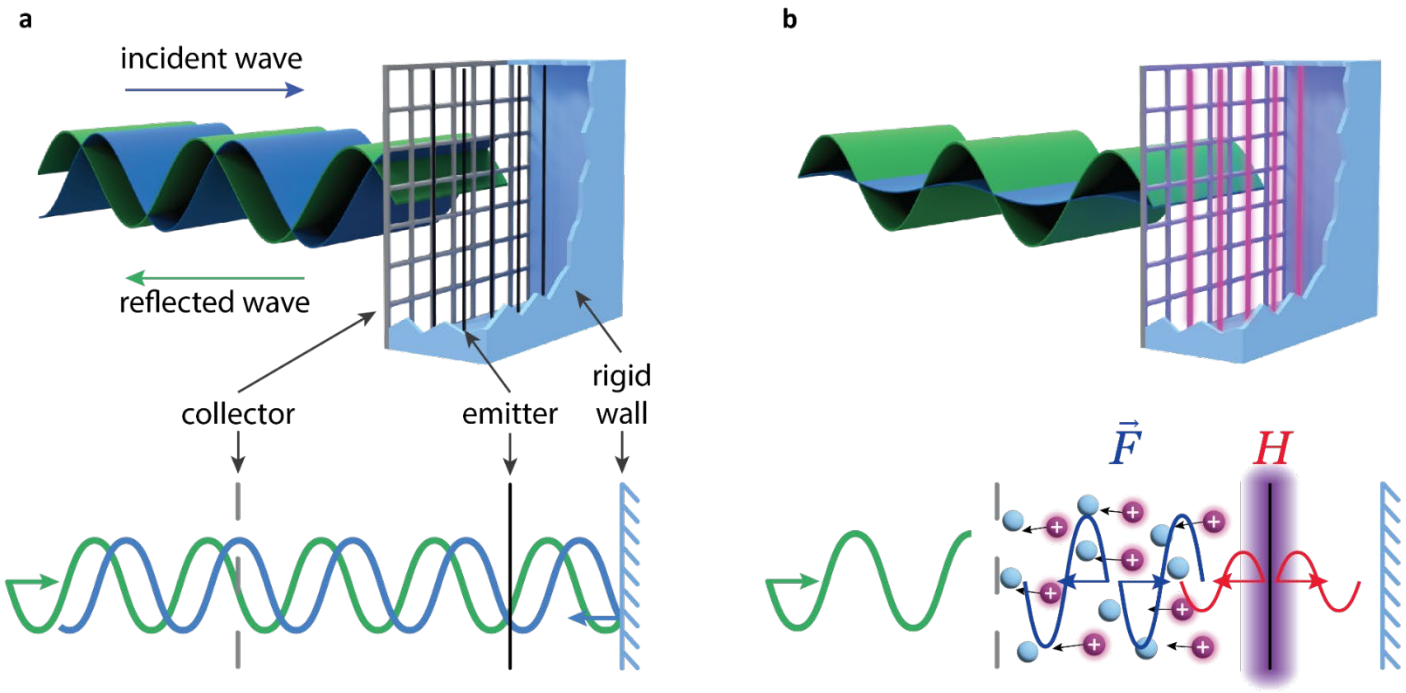

Principle of sound absorption with CD in closed box

Analytical control transfer function

1D wave equation

$$\left(\frac{\partial^2}{\partial x^2} + k^2\right) p = -\frac{j\omega}{C_P T_0} h + \frac{\partial f}{\partial x}$$

CD sound sources

$$H = hSd = C(3U_{DC}^2 - 2U_{DC}U_0)u_{AC}$$

$$F = fSd = \frac{Cd}{\mu_i}(2U_{DC} - U_0)u_{AC}$$

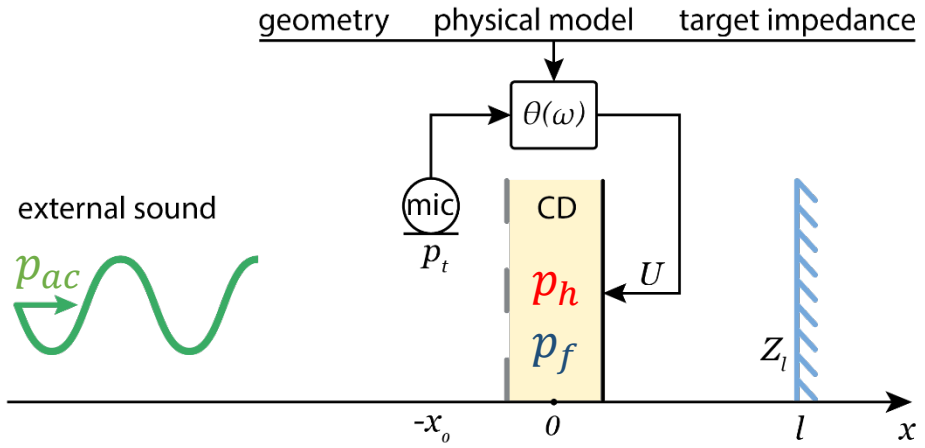

1D schematic of acoustic sources and boundaries positions

Total acoustic field is a sum

$$p_t(x) = p_f(x) + p_h(x) + p_{ac}(x)$$

$$v_t(x) = v_f(x) + v_h(x) + v_{ac}(x)$$

$$Z_{tg}(-x_0) = \frac{p_t(-x_0)}{v_t(-x_0)}$$

$$Z_{ac}(-x_0) = \frac{p_{ac}(-x_0)}{v_{ac}(-x_0)} = \rho c \frac{Z_l + j\rho c \tan(k(l + x_0))}{\rho c + jZ_L \tan(k(l + x_0))}$$

Control TF

$$\theta = \frac{u_{AC}}{p_t(-x_0)}$$

Original vs control transfer function

Analytical transfer function

$$\theta = \frac{1}{A}\left(1 - \frac{Z_{ac}}{Z_{tg}}\right) / \left(1 + \frac{Z_{ac}}{\rho c}\right)$$

$$A = \frac{d}{2}\left[\left(f_0 + \frac{ch_0}{C_P T_0}\right)\exp(-jkx_0) + \left(-f_0 + \frac{ch_0}{C_P T_0}\right) r \exp(-jk(x_0 + 2l))\right]$$

Control transfer function

$$\theta = \frac{\theta_1}{\theta_2}, \quad \theta_1 = \frac{\left(Z_l - \frac{\rho c}{n}\right)\left(\frac{n\rho c - Z_l}{nZ_l - \rho c} + \frac{ls}{c}\right)}{(Z_l + \rho c)\left(1 + \frac{ls}{c}\right)}$$

$$\theta_2 = f_0 + \frac{ch_0}{C_P T_0} + \left(-f_0 + \frac{ch_0}{C_P T_0}\right) r \frac{1 - \frac{ls}{c} + \frac{l^2}{2c^2}s^2}{1 + \frac{ls}{c} + \frac{l^2}{2c^2}s^2}$$

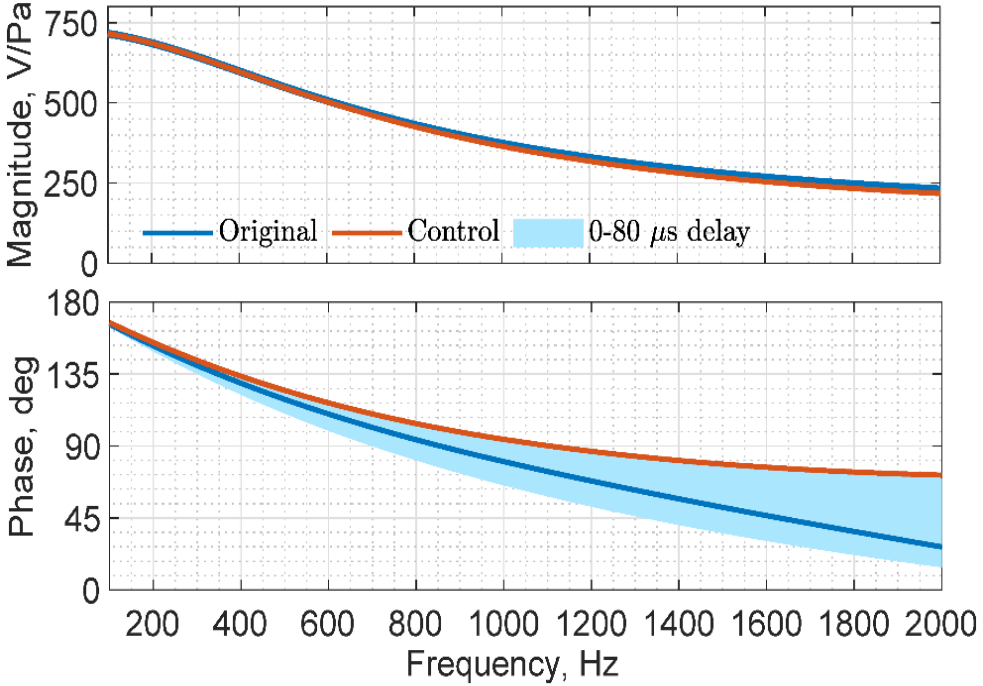

Bode plots of analytical and control transfer functions

$$f_0 = \frac{f}{u_{AC}} = \frac{C}{S\mu_i}(2U_{DC} - U_0)$$

$$h_0 = \frac{h}{u_{AC}} = \frac{C}{Sd}(3U_{DC}^2 - 3U_{DC}U_0)$$

Modelling CD control with different time delays

- Low sound absorption at high frequencies due to mismatch in phase
- Performance improves with additional time delay to control output
- Total delay should not be higher than 80 μs

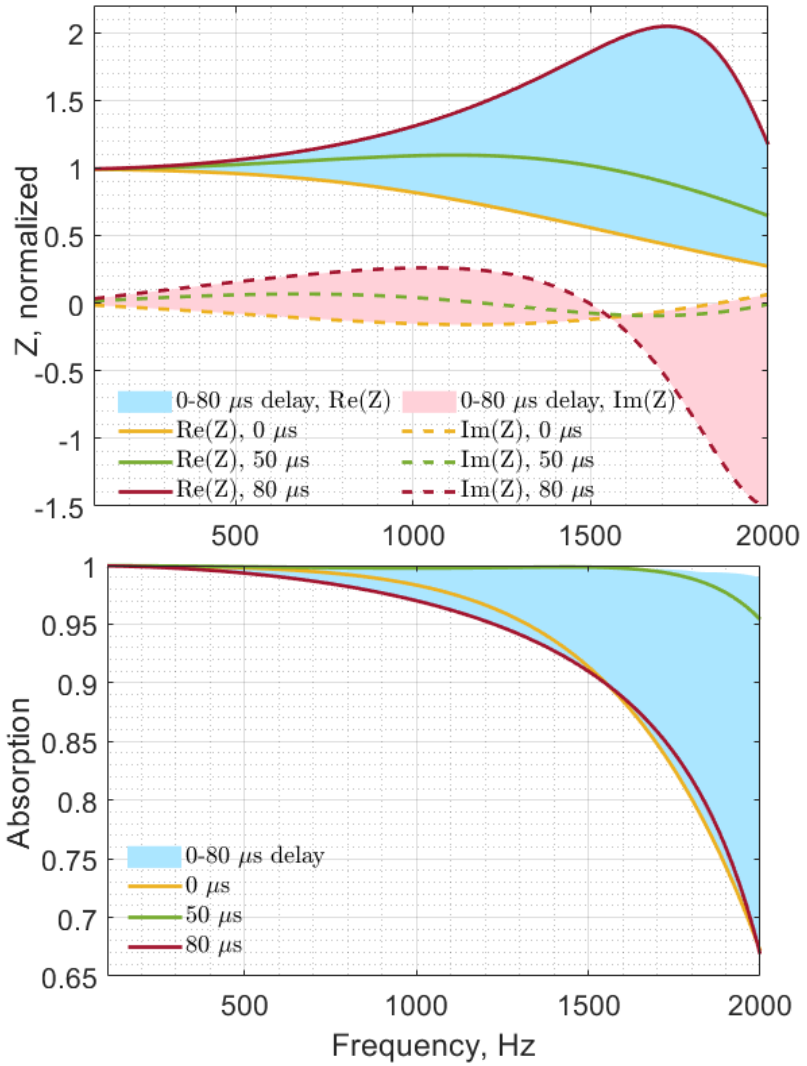

Simulated acoustic impedance and absorption coefficient

Optimal time delay for improving CD sound absorption

- 50 μs delay leads to highest overall absorption in 100-2000 Hz
- Optimal delay depends on target impedance

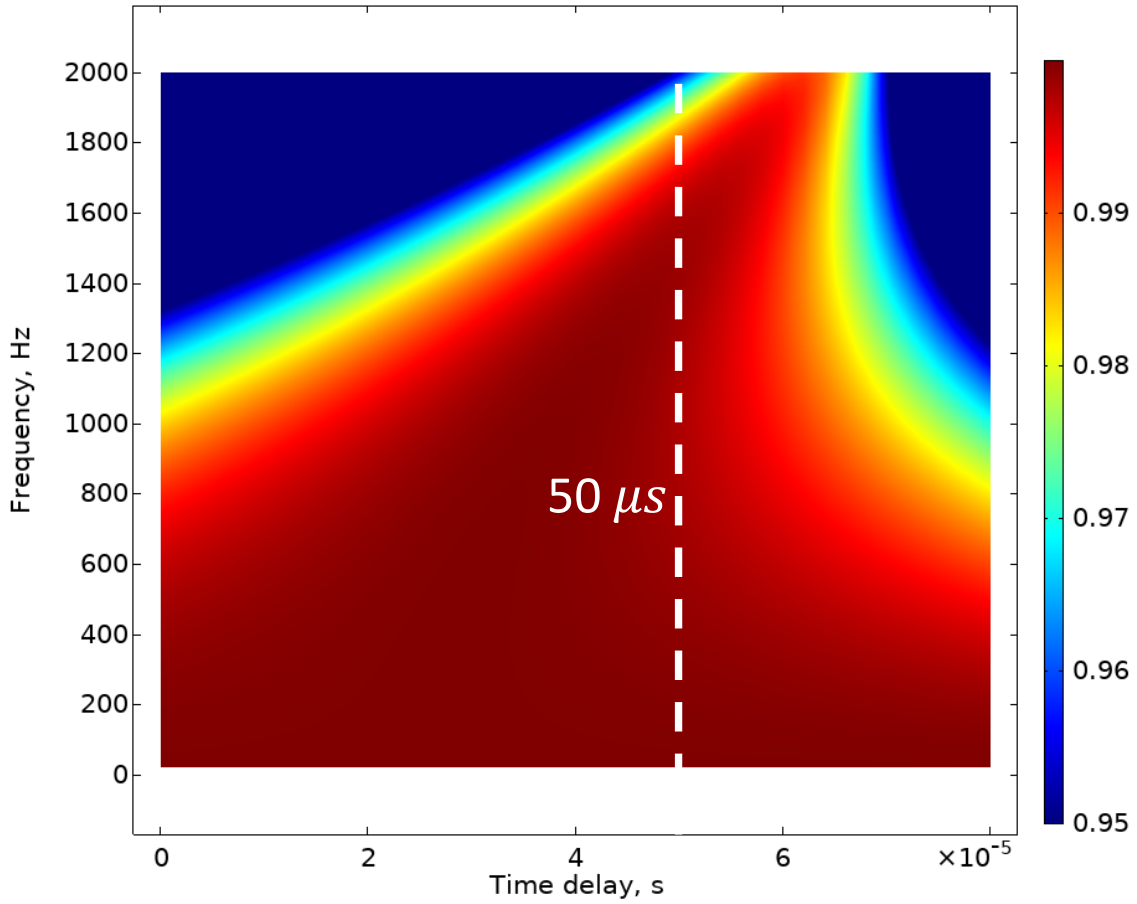

Absorption coefficient map as function of frequency and control time delay

Experimental validation

Physical setup:

- $M_r = M_2$ - reference mic, measures noise to absorb
- p_t - control microphone
- M_1 and M_2 - to measure impedance and absorption
- Hard wall at 2 cm after corona

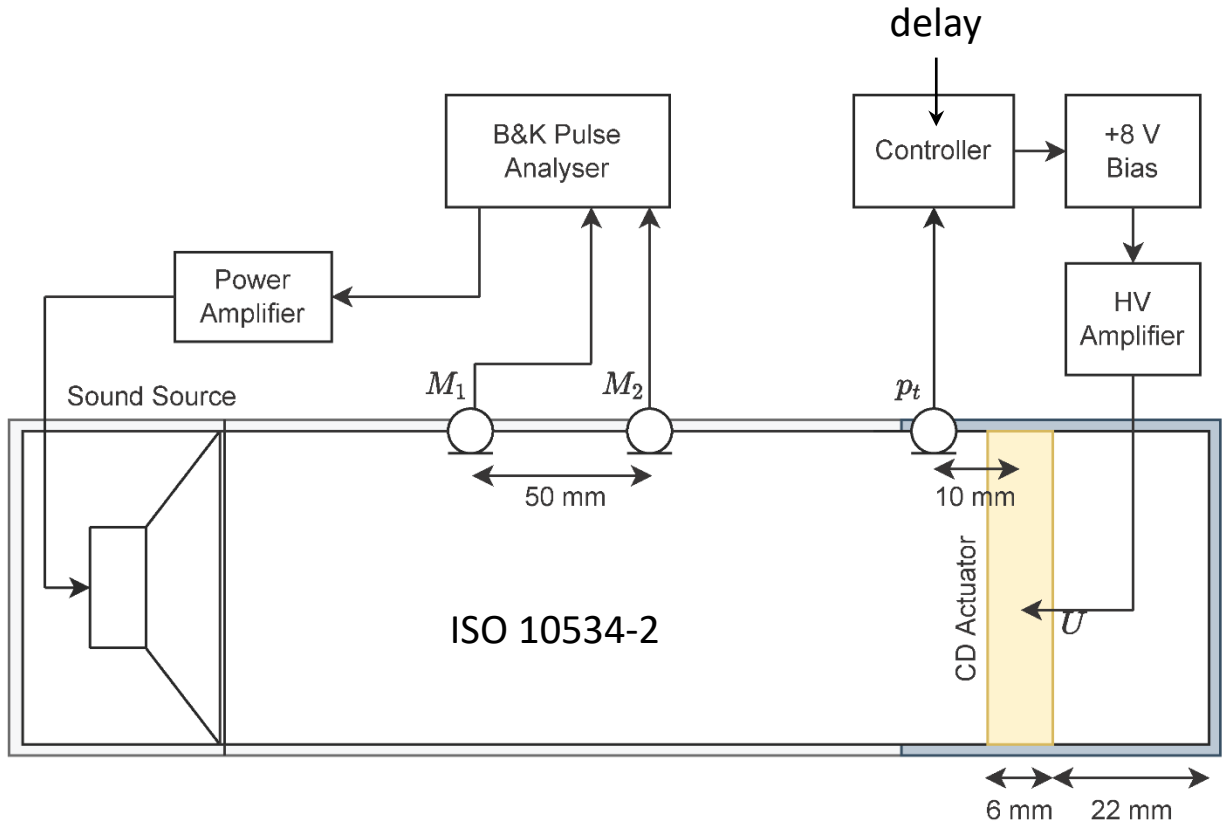

Schematic of experimental setup

- HV amplifier delay ~14 μs
- Controller time delay ~18 μs

Broadband sound absorption

Passive measurement

- Low constant absorption due to hard wall
- Z_l as constant real impedance works well

Active CD with ~30 μs delay

- Perfect absorption at low frequencies
- Deviation from Z_{tg} from 1 kHz
- Good match with simulation

Active CD with ~50 μs delay

- Perfect absorption extended
- >95% absorption up to 2 kHz

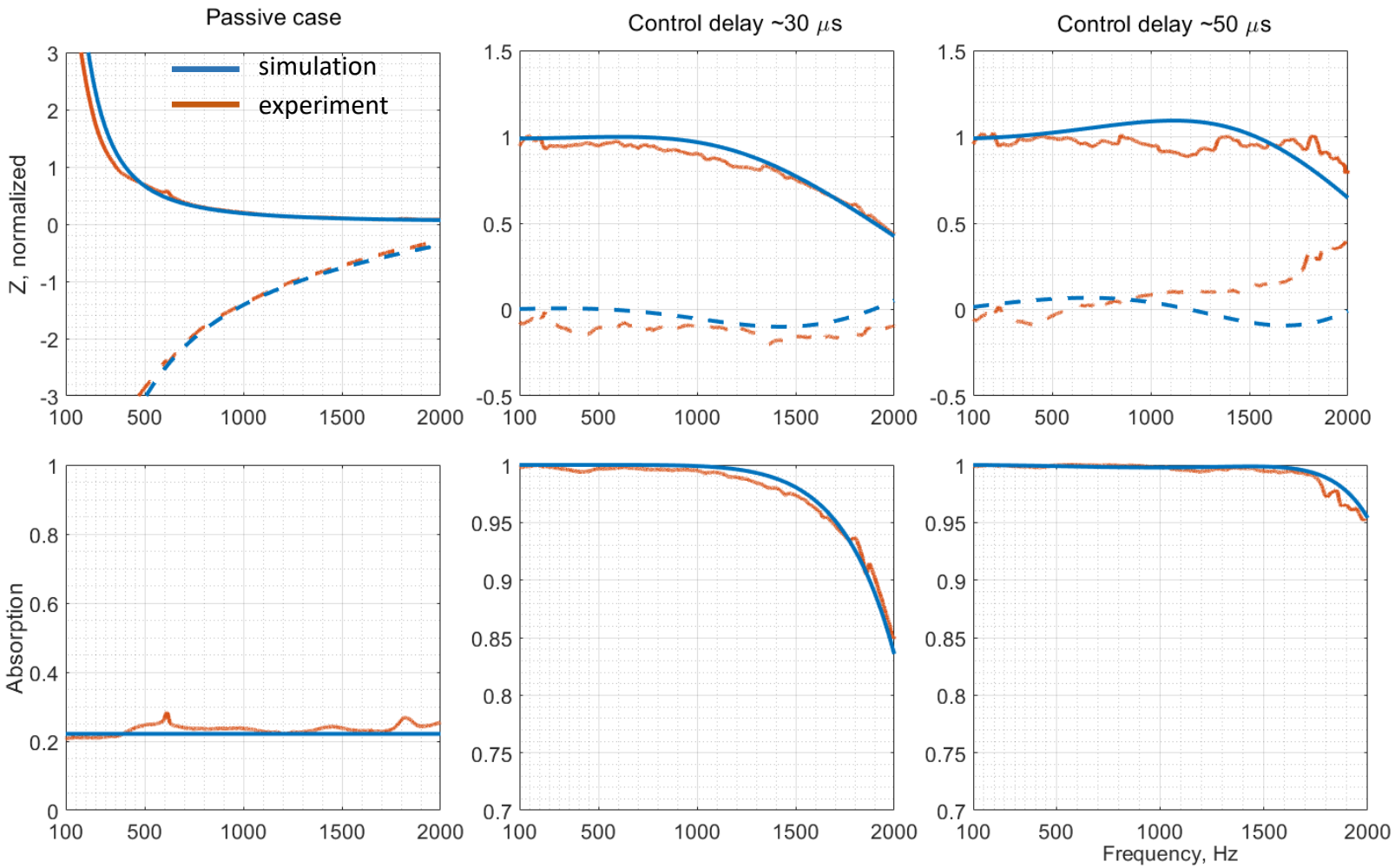

Schematic of experimental setup

Broadband sound absorption

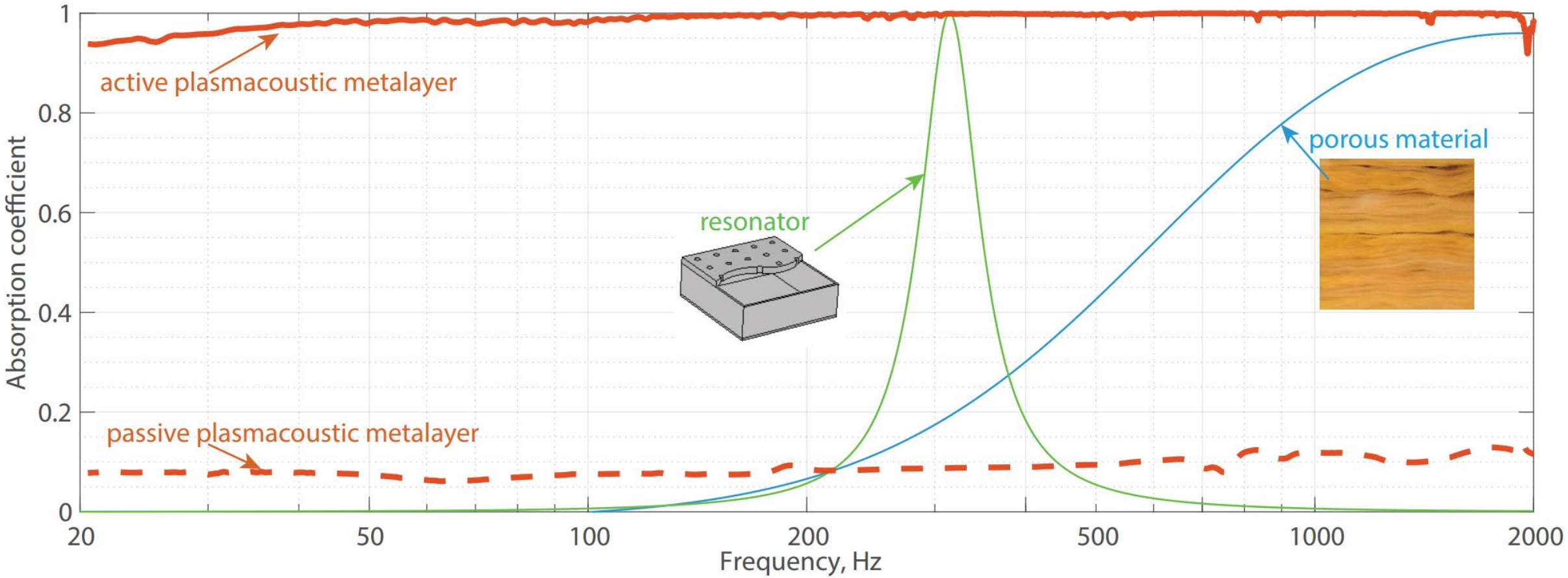

Introducing delay in a reflected wave

Implementation

- Target impedance is similar to passive Z_{AC}
- Virtually mimics longer duct behind CD (+ l_1)

Result

- Can change the angle of reflection phase
- Corresponds to different constant delay in reflected wave
- Can change magnitude/phase of reflection independently

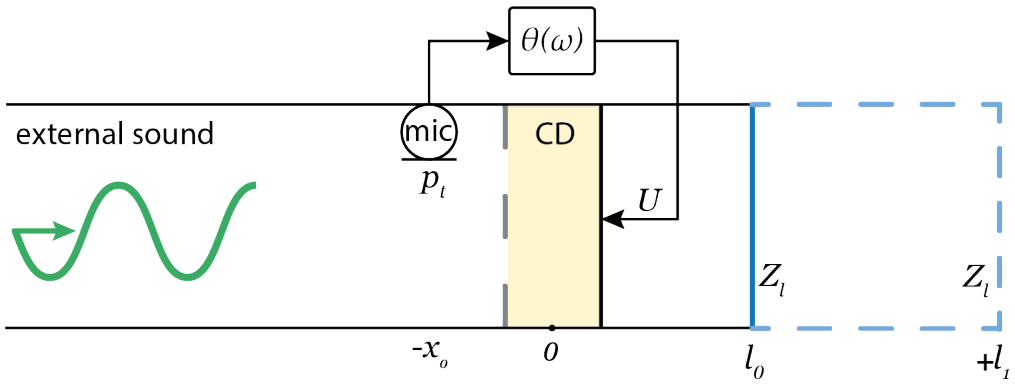

$$Z_{tg} = \rho c \frac{\beta Z_l + j\rho c \tan\left(k(l_0 + l_1 + x_0)\right)}{\rho c + j\beta Z_l \tan(k(l_0 + l_1 + x_0))}$$

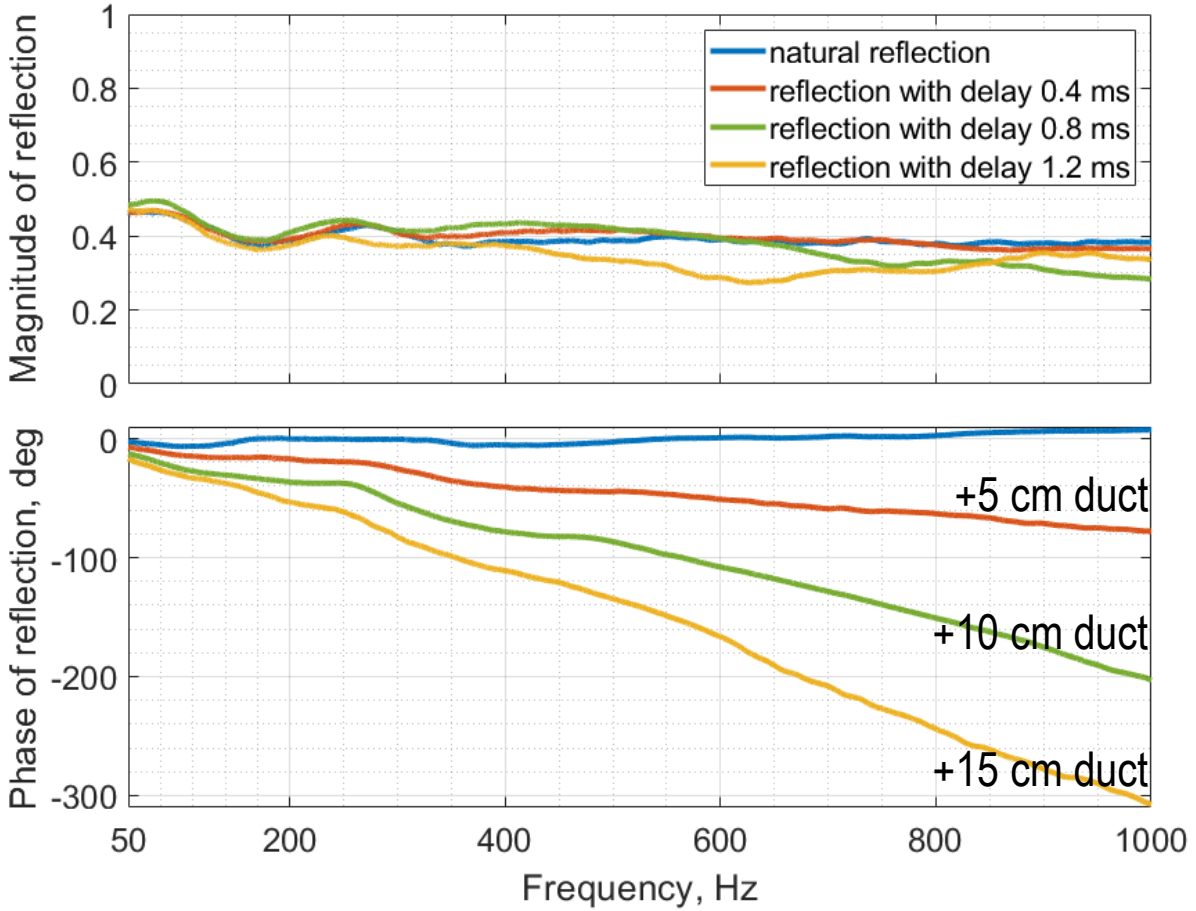

Adjustable absorption coefficient of controlled CD actuator

Current limitations

- Depending on application different control strategy can be preferable
- Low sound pressure level of operation
- High voltage signal amplification
- Possible transition to arc
- Ozone generation

Merci !

Noise sources in aircraft

Noise sources:

- Airplane frame
- Engine

Advances in noise reduction:

- High by-pass ratio engines
- Novel plane frame

Engine needs further noise reduction

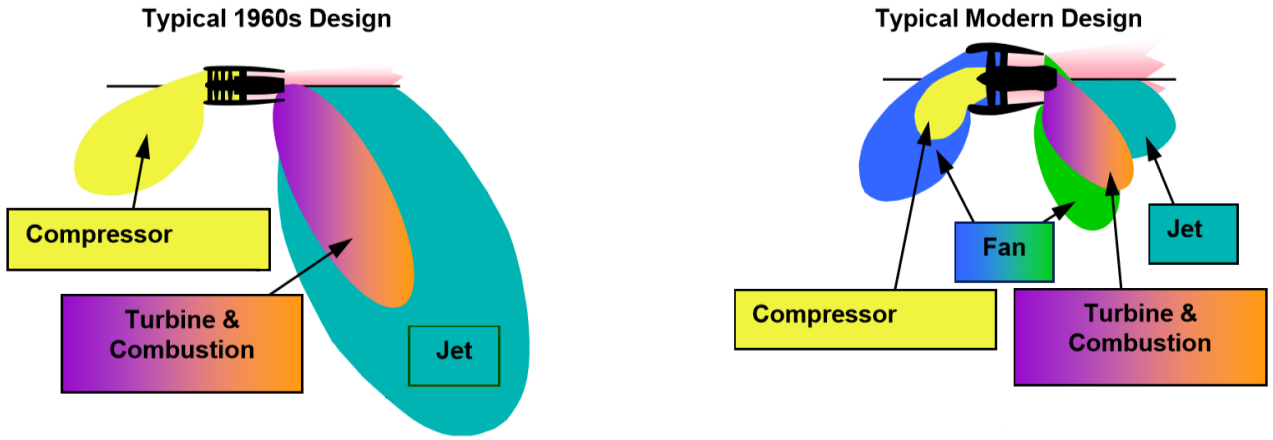

Noise diagrams from different engine parts

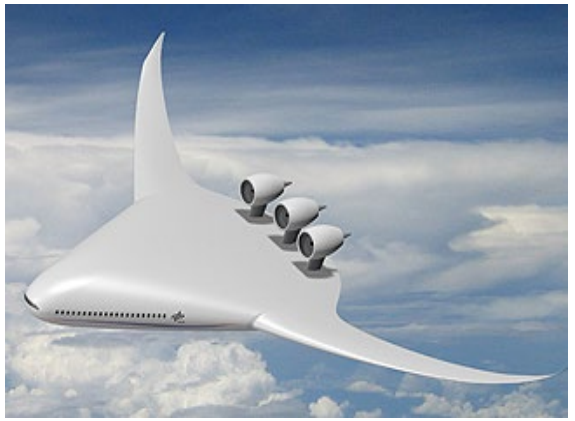

Blended wing body concept

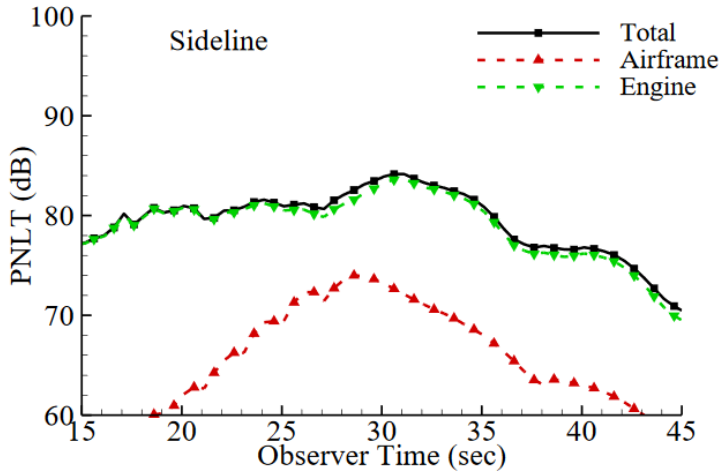

Noise level at observer point [1]

[1]. Gou Y., Russell H. T. System Noise Assessment of Blended-Wing-Body Aircraft with Open Rotor Propulsion. 2015. NASA report.

Varying absorption/reflection level

Implementation

- Target impedance mimics passive Z_{AC}
- Adjustable termination rigidity βZ_L

Result

- Tuneable absorption/reflection amount
- Broadband behaviour

$$Z_{tg} = \rho c \, \frac{\beta Z_L + j\rho c \tan\left(k(L + x_0)\right)}{\rho c + j\beta Z_L \tan(k(L + x_0))}$$

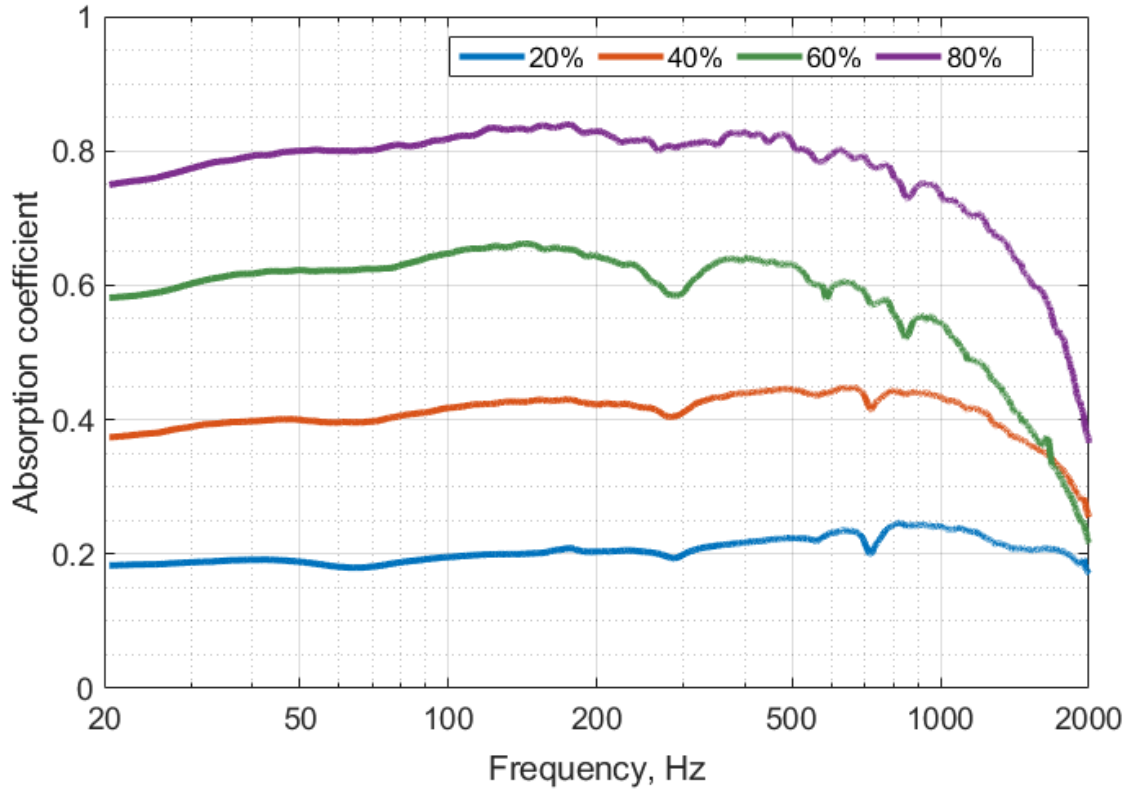

Adjustable absorption coefficient of controlled CD actuator

High voltage amplifier prototype

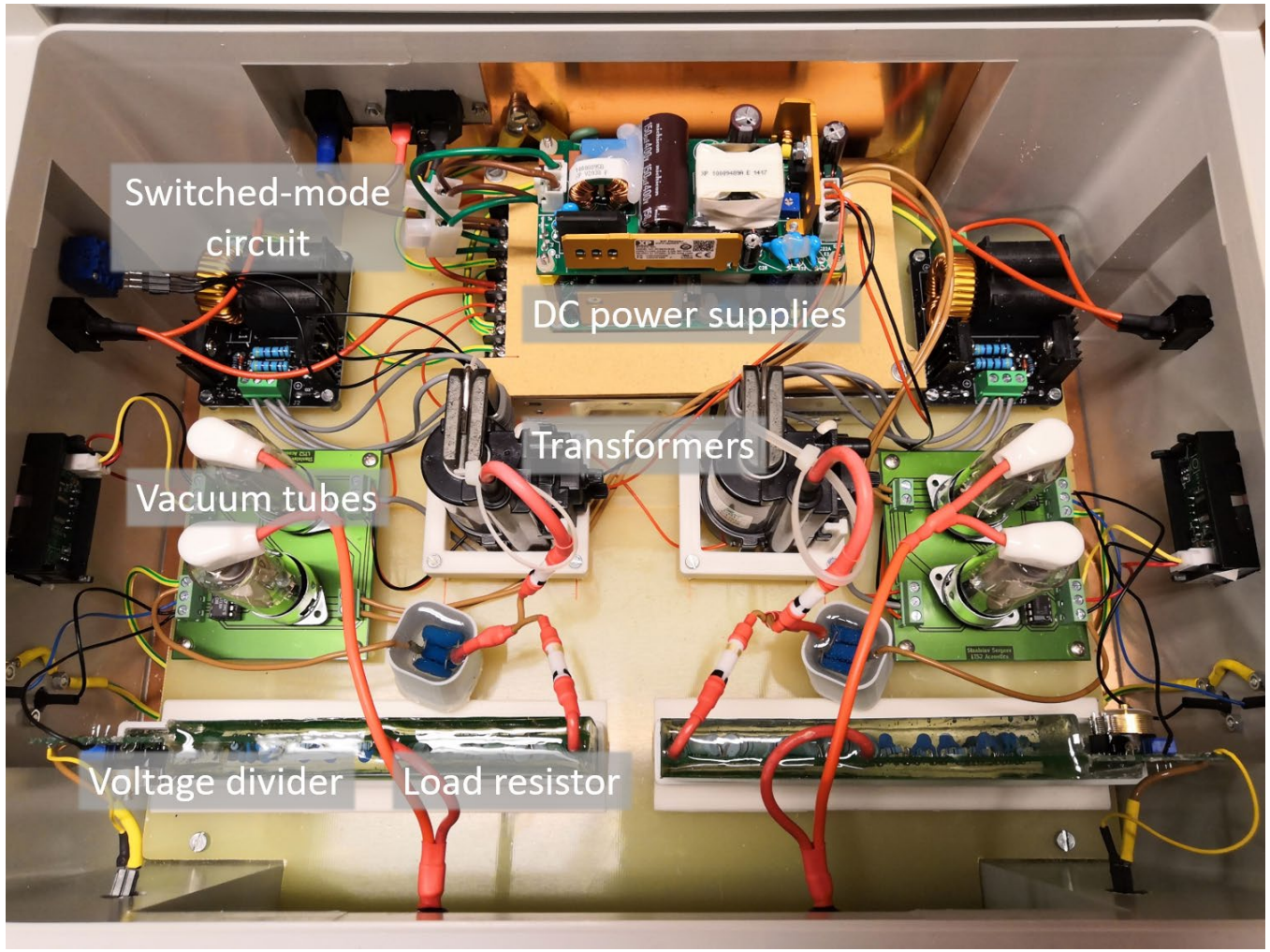

Derivation of control transfer function

$$\left(\frac{\partial^2}{\partial x^2}+k^2\right)p=-\frac{j\omega}{C_P T_0}h+\frac{\partial f}{\partial x}$$

$$p_h=\frac{dc}{2C_P T_0}h\left(\exp(jkx)+r\exp\left(jk(x-2L)\right)\right)$$

$$v_f=-\frac{d}{2\rho c}f\left(\exp(jkx)-r\exp\left(jk(x-2L)\right)\right)$$

$$p_h=\frac{dc}{2C_P T_0}h\left(\exp(jkx)+r\exp\left(jk(x-2L)\right)\right)$$

$$v_h=-\frac{d}{2\rho C_P T_0}h\left(\exp(jkx)+r\exp\left(jk(x-2L)\right)\right)$$

$$p_t=p_f+p_h+p_{ac}$$

$$v_t=v_f+v_h+v_{ac}$$

$$Z_{ac}=\rho c\frac{Z_L+j\rho c\tan(kL)}{\rho c+jZ_L\tan(kL)}$$

$$v_t=v_f+v_h+\frac{p_t-p_f-p_h}{Z_{ac}}$$

$$Z_{tg}=p_t/v_t$$

$$\theta=\frac{1}{A}\left(1-\frac{Z_{ac}}{Z_{tg}}\right)$$

$$A=\frac{d}{2}\left(1+\frac{Z_{ac}}{\rho c}\right)\left[\left(f_0+\frac{ch_0}{C_P T_0}\right)\exp(jkx_0)+\left(-f_0+\frac{ch_0}{C_P T_0}\right)r\exp\left(jk(x_0-2L)\right)\right]$$

Results

Can achieve broadband absorption

Tunable control configuration for absorption in different conditions

Can be controlled in a classical feedback manner

Scalable in size without change in a response

Transparent, thin, lightweight for new applications

Near acoustic field

- High pressure regions around the emitter wires
- Uniform pressure along the collector grid

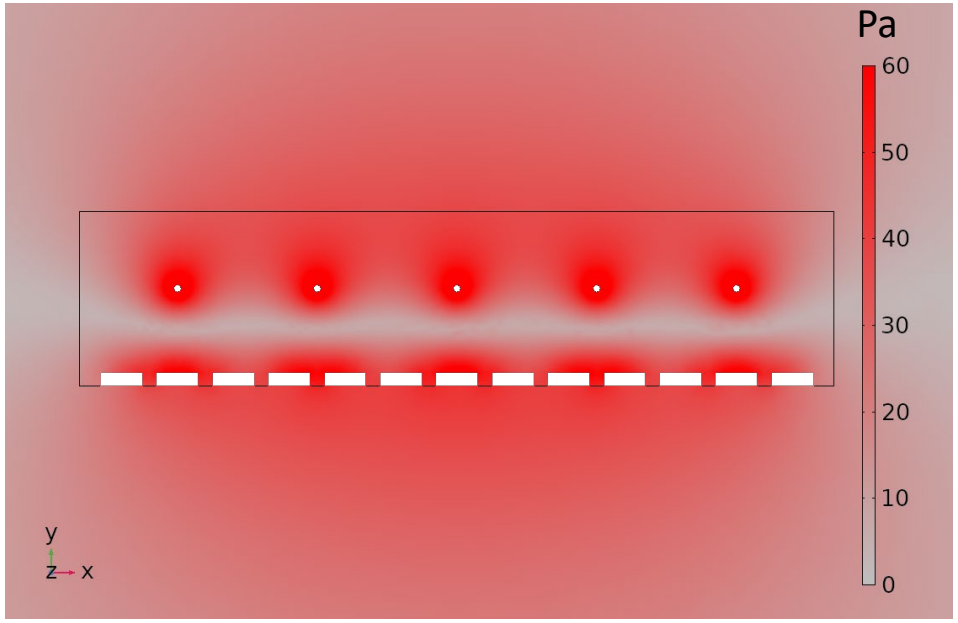

Pressure distribution around the electrodes

Voltage-current characteristics comparison

Observations

- In general model captures the I(U) trend
- Numerical model slope is less steep
- Lowest error around 8 kV~ U_{DC} (10% at u_{AC}=800V)

Reasons

- 2D geometry approximation
- Discharge parameters (μ_i) from literature

For analytical model

- Least-squares fit to obtain C and U_0

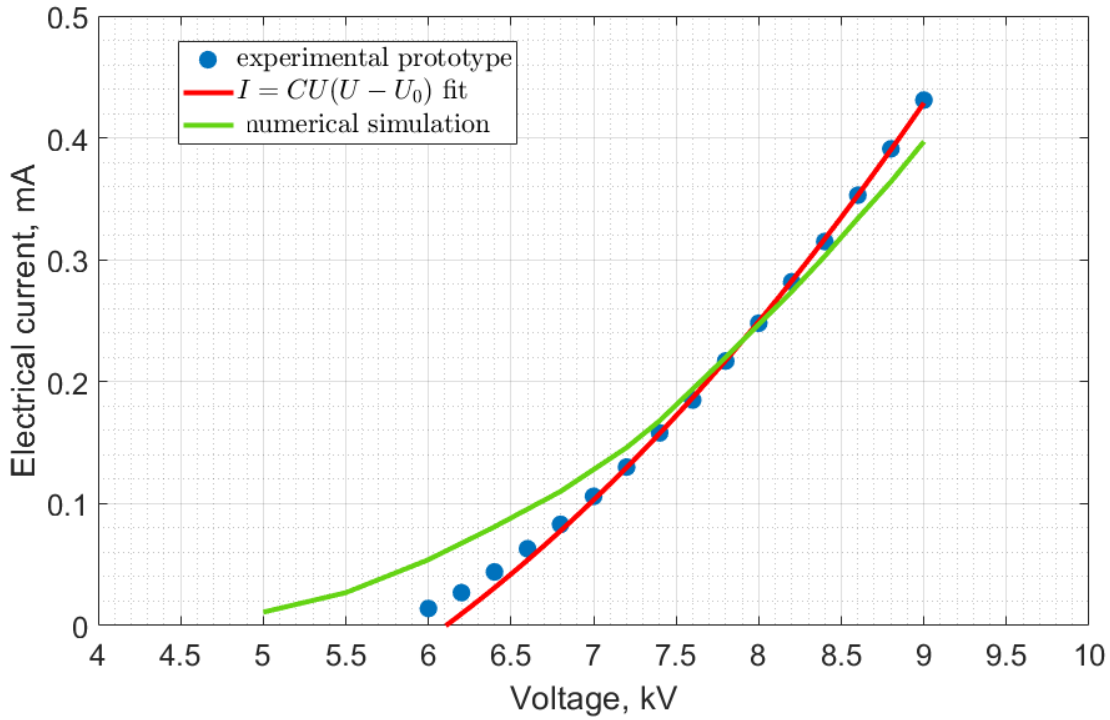

I(U) curve comparison and fit for analytical model